# Estimation of light penetration, and horizontal and vertical visibility in oceanic and coastal waters from surface reflectance

Maeva Doron, Marcel Babin, Antoine Mangin, Odile Hembise

# Estimation of light penetration, and horizontal and vertical visibility in oceanic and coastal waters from surface reflectance

Maéva Doron,[1,2,3] Marcel Babin,[2,3] Antoine Mangin,[1] and Odile Hembise[1]

Received 9 November 2006; accepted 24 January 2007; published 5 June 2007.

[1] We present algorithms for the estimation of the vertical diffuse attenuation coefficient, $K_d$ ($m^{-1}$), and the beam attenuation coefficient, $c$ ($m^{-1}$), at 490 nm from irradiance reflectance. Our aim is to retrieve as analytically as possible $[K_d(490) + c(490)]^{-1}$, a proxy for vertical visibility. The two algorithms are based on the semianalytical retrieval of the absorption coefficient $a$ ($m^{-1}$) and the backscattering coefficient $b_b$ ($m^{-1}$) from reflectance at two wavelengths, 490 and 709 nm. The use of a near-infrared wave band allows a small number of simple assumptions to be made, (1) light absorption at 709 nm is only due to pure seawater, and (2) there exists a constant ratio between the particulate backscattering coefficients at 490 and 709 nm. To estimate $c(490)$, we developed an empirical relationship between $b$ and $b_b$ for particles. Algorithm development, testing, and validation are achieved using data from the literature, a synthetic data set, and a large in situ data set of inherent and apparent optical properties measured in various environments. The algorithms are found to be valid both in coastal and oceanic waters, and largely insensitive to regional peculiarities in the inherent optical properties. The values of $K_d(490)$ and $c(490)$ are retrieved within a factor of 2.21 and 2.91 (95% confidence interval), respectively, using independent in situ data sets. This performance for $K_d(490)$ is better or comparable to that of recently published algorithms. This study opens the way to the development of simple semianalytical ocean color algorithms that make the best use of spectral information.

**Citation:** Doron, M., M. Babin, A. Mangin, and O. Hembise (2007), Estimation of light penetration, and horizontal and vertical visibility in oceanic and coastal waters from surface reflectance, *J. Geophys. Res.*, *112*, C06003, doi:10.1029/2006JC004007.

## 1. Introduction

[2] The spectral attenuation of solar radiation in the ocean by seawater and its constituents determines the vertical distribution of light, which in turn impacts on photochemical reactions such as photosynthesis and photo oxidation, and determines the vertical distribution of heat deposition. Light attenuation also affects in-water visibility of animals and humans.

[3] Various quantities have been used in optical oceanography for describing the attenuation of light. The most common ones are the vertical diffuse attenuation coefficient, $K_d$ ($m^{-1}$), which describes the attenuation of the planar irradiance along the vertical, and the beam attenuation coefficient, $c$ ($m^{-1}$), which describes the attenuation of a collimated beam of light. Horizontal visibility is closely related to the inverse of $c$ [*Zaneveld and Pegau*, 2003], while vertical visibility, analogous to the Secchi disk depth, is well described by the inverse of the sum $K_d + c$ [*Tyler*, 1968] (see Table 1 for a list of symbols and subscripts).

[4] The estimation of $K_d$ from remotely sensed surface reflectance was introduced by *Austin and Petzold* [1981] for open ocean (so-called case 1 [*Morel and Prieur*, 1977]) waters. Their algorithm consists of an empirical relationship between $K_d(490)$ and a blue-to-green radiance ratio, for instance $L_u(443)/L_u(550)$, where $L_u(\lambda)$ is the subsurface spectral upwelling radiance (W $m^{-2}$ $sr^{-1}$ $nm^{-1}$) and $\lambda$ is the wavelength (nm). This algorithm, revisited by *Mueller* [2000], is now routinely applied in the data processing of several ocean color satellite sensors (for example, the NASA sensors SeaWiFS and Moderate-Resolution Imaging Spectroradiometer).

[5] In coastal (so-called case 2 [*Morel and Prieur*, 1977]) waters, the empirical algorithms valid for open ocean waters show poor performances [*Lee et al.*, 2005a]. For a given value of $L_u(443) / L_u(550)$, various values of $K_d(490)$ can be found. One reason at the origin of this problem is that the concentrations of the different optically significant substances present in seawater covary poorly in case 2 waters, compared with case 1 ones, and affect $L_u(443) / L_u(550)$ and $K_d$ in different manners. These substances, generally partitioned into three components, phytoplankton, nonalgal particles (NAP), and colored dissolved organic matter (CDOM), originate not only from autochthonous biological

[1] ACRI-ST, 260 route du Pin Montard, Sophia Antipolis, France.
[2] Laboratoire d'Océanographie de Villefranche, Université Pierre et Marie Curie-Paris6, Villefranche-sur-Mer, France.
[3] Laboratoire d'Océanographie de Villefranche, CNRS, Villefranche-sur-Mer, France.


0148-0227/07/2006JC004007

**Table 1.** List of Symbols, Units, and Subscripts

| Symbol | Description | Unit |
|---|---|---|
| $a(\lambda)$ | Absorption coefficient | $m^{-1}$ |
| $b(\lambda)$ | Scattering coefficient | $m^{-1}$ |
| $b_b(\lambda)$ | Backscattering coefficient | $m^{-1}$ |
| $\tilde{b}_{bp}(\lambda)$ | Backscattering efficiency for the particles | Dimensionless |
| $B_{490-709}$ | Average ratio of the scattering coefficient at 490 and 709 nm | Dimensionless |
| $c(\lambda)$ | Beam attenuation coefficient | $m^{-1}$ |
| $c(v)$ | Photopic beam attenuation coefficient | $m^{-1}$ |
| $C_0$ | Inherent contrast between the disk and background water | Dimensionless |
| $C_{min}$ | Minimum apparent contrast perceivable by the human eye | Dimensionless |
| $E_d(\lambda, z)$ | Downward plane irradiance at the depth $z$ | W $m^{-2}$ $nm^{-1}$ |
| $E_u(\lambda, z)$ | Upward plane irradiance at the depth $z$ | W $m^{-2}$ $nm^{-1}$ |
| $f(\lambda)$ | Proportionality factor between $R(\lambda)$, $b_b(\lambda)$, and $a(\lambda)$ with $R(\lambda) = f(\lambda)\frac{b_b(\lambda)}{a(\lambda)}$ | Dimensionless |
| $f'(\lambda)$ | Proportionality factor between $R(\lambda)$, $b_b(\lambda)$, and $a(\lambda)$ with $R(\lambda) = f'(\lambda)\frac{b_b(\lambda)}{a(\lambda)+b_b(\lambda)}$ | Dimensionless |
| $K_d(\lambda)$ | Vertical diffuse attenuation coefficient | $m^{-1}$ |
| $K_d(v)$ | Photopic vertical diffuse attenuation coefficient | $m^{-1}$ |
| $L_u(\lambda, \theta, \varphi, z)$ | Upwelling radiance in the viewing direction | W $m^{-2}$ $sr^{-1}$ $nm^{-1}$ |
| $L_w(\lambda, 0^+)$ | Water-leaving radiance in the viewing direction | W $m^{-2}$ $sr^{-1}$ $nm^{-1}$ |
| $n_1$ or $n_2$ | Parameter for the spectral dependency of the scattering coefficients in the IOCCG data set | Dimensionless |
| $Q$ | Bidirectionality factor | Dimensionless |
| $R(\lambda)$ | Irradiance reflectance just below the surface | Dimensionless |
| $R_{rs}(\lambda)$ | Above-surface remote-sensing reflectance | $sr^{-1}$ |
| $r_{rs}(\lambda)$ | Below-surface remote-sensing reflectance | $sr^{-1}$ |
| $\theta_S$ | Zenith solar angle | ° |
| $Z_{SD}$ | Secchi disk depth | m |
| **Subscript** | **Signification** | |
| No subscript | Total | |
| $p$ | Particulate (in the meaning of suspended particulate material) | |
| $w$ | Water | |
| ^ | Estimated variable, for example, $\hat{K}_d$ | |

production but also from exogenous sources through river discharge and from resuspension of bottom sediment.

[6] To circumvent the difficulties encountered in case 2 waters when interpreting ocean color, hyperspectral approaches have been proposed during the 1990s, in which a forward reflectance model is built essentially through parameterizing the spectral shapes of the absorption and scattering coefficients of the optically significant seawater components, to reproduce as well as possible the natural reflectance [e.g. *Lee and Carder*, 1994]. The inverse model consists in minimizing the difference between the measured and simulated reflectance spectra by varying the magnitude of the IOPs. Algorithms based on this approach have been proposed for the retrieval of $a$, the backscattering coefficient ($b_b$; $m^{-1}$), and $c$, in case 1 and case 2 waters [e.g. *Roesler and Perry*, 1995; *Roesler and Boss*, 2003; *Lee and Carder*, 1994; *Lee et al.*, 1996]. From a remote sensing perspective, the use of hyperspectral algorithms is currently impeded by the lack of hyperspectral spaceborne ocean color sensors. This may change in the near future as projects for experimental hyperspectral sensors are emerging. With regard to operational missions, however, the near future as the VIIRS sensor designed for the future North Polar Operational Environmental Satellite System (NPOESS, NOAA, expected launch date 2009) and the future Sentinel operational mission of the European Space Agency (expected launch date 2010) will both offer a limited number of spectral bands in the visible for ocean color remote sensing.

[7] Because the optical properties of seawater strongly covary between wavelengths [e.g. *Gould et al.*, 1999; *Babin et al.*, 2003b], most variability in reflectance can be explained using less than five spectral channels [*Sathyendranath et al.*, 1989]. However, a major problem encountered when attempting to invert reflectance spectra in complex natural waters is one of ambiguity; more than one combination of IOPs can produce nearly the same reflectance spectrum [*Sydor et al.*, 2004; *Defoin Platel and Chami*, 2006]. To avoid as much as possible that problem, perhaps more acute for algorithms that use only few spectral bands, spectral domains where useful and unambiguous information is found must be identified and used, within and beyond the blue and green domains generally used by ocean color algorithms.

[8] In this study, we propose alternative algorithms for retrieving the total $a$ and $b_b$ at 490 nm that use the reflectance signal at two wavelengths only and is based on simple analytical expressions in which the parameters are measurable quantities obtained from the literature. The two wavelengths are 490 nm, where both absorption and scattering by all seawater optical components are significant and contribute to variability in reflectance, and 709 nm where variations in reflectance are almost solely due to changes in the particle backscattering coefficient. On the basis of these $a$ and $b_b$ algorithms, we (1) use a robust relationship derived by *Lee et al.* [2005a] to retrieve $K_d(490)$ and (2) propose an algorithm to retrieve $c(490)$ that uses an empirical relationship between the backscattering and scattering coefficients for particles. Additionally, we use 1 and 2 to retrieve the vertical visibility as expressed by $[K_d(490) + c(490)]^{-1}$. This development leads to a semianalytical algorithm allowing us to retrieve the vertical visibility using two wave bands.

[9] The algorithms to estimate $a$ and $b_b$ are parameterized using values obtained from the literature and thus independently from any of the data sets used in this study. The robustness of the algorithm to retrieve $K_d(490)$ is tested with an artificial data set and validated using a data set obtained in European coastal waters and consisting of more than 400 simultaneous measurements of IOPs and apparent optical properties (AOPs; $R$ and $K_d$). Because the latter data set is also used to adjust the parameters of our $c(490)$ algorithm, this algorithm was also validated using a different in situ data set.

## 2. Material and Methods

[10] In order to parameterize and test our algorithms, we used three separate data sets. The first data set was generated through radiative transfer simulations and excludes measurement errors. The second set is a large bio-optical database that includes IOPs and AOPs obtained in European coastal waters. The third data set is used to provide a validation and was obtained from various locations.

### 2.1. IOCCG Case 2 Waters Reference Data Set

[11] A reference set of synthetic optical data created by the Working Group on Ocean Color Algorithms of the International Ocean Color Coordinating Group [*IOCCG*, 2006; *Lee et al.*, 2005b] was used in the present study to assess our algorithms. This data set, thereafter referred to as the IOCCG data set, consists of 1000 simulations (500 combinations of IOPs times two solar angles) obtained from radiative transfer calculations made using the Hydrolight© code (Sequoia Scientific Inc., Redmond WA, USA). The main features of the IOCCG data set relevant to the present study are the following: the IOPs were varied separately for the three optically significant components NAP, CDOM, and phytoplankton within ranges and proportions representative of natural waters, over the visible and near-infrared (near-IR) range (every 10 nm between 400 and 800 nm). The variations of the beam attenuation coefficient of phytoplankton follow a $\lambda^{-n_1}$ spectral dependency with $n_1$ randomly varying between $-0.1$ and 2. The variations of the NAP scattering coefficient follow a $\lambda^{-n_2}$ spectral dependency with $n_2$ randomly varying between $-0.2$ and 2.2. A Fournier-Forand scattering phase function with a backscattering-to-scattering ratio of 1% [*Fournier and Forand*, 1994] was used for phytoplankton while the phase function proposed by *Mobley et al.* [1993] was used for the pool of other particles. The calculations were made for two different solar angles (30° and 60°). The data set and a description of the procedure used to create it are available at http://www.ioccg.org/groups/OCAG_data.html. In this study, we used the subsurface data for the $R(490)$, $R(710)$, and $K_d(490)$. The values of $c(490)$ were evaluated from the input IOPs.

### 2.2. COASTlOOC Data Set

[12] During the COASTlOOC project, seven campaigns were conducted to measure IOPs and AOPs and related chemical seawater properties (see the detailed description in the work by *Babin et al.* [2003a, 2003b]). Different types of case 2 waters were sampled in the Mediterranean Sea, Baltic Sea, North Sea, English Channel, and Adriatic Sea. Case 1 waters were also sampled in the Atlantic Ocean and Mediterranean Sea. A total of 424 locations were visited in more than 15 river plumes and other coastal and open ocean environments. Measurements were carried out from a helicopter (233 stations) and from a ship (191 stations).

[13] In this study, we use the absorption and attenuation coefficients data measured in-water at nine wavelengths using an ac-9 profiler (WET Labs Inc., Philomath OR, USA). Owing to the ac-9 calibration protocol, these coefficients exclude the contribution of pure seawater. They are therefore denoted $a$-$a_w$ and $c$-$c_w$, respectively. The difference between the measured ($c$-$c_w$) and ($a$-$a_w$) coefficients yields the scattering coefficient by particles, $b$-$b_w$, later denoted $b_p$ (detailed measurement protocol described in the work by *Babin et al.* [2003b]). The absorption coefficient was also spectrophotometrically determined from 380 to 750 nm (1-nm increment) on seawater samples, separately for phytoplankton, nonalgal particles, and CDOM as described in the work by *Babin et al.* [2003a].

[14] We also use the $K_d$ and $R$ data derived from in-water radiometric measurements performed during the COASTlOOC campaigns. Vertical profiles of downward and upward irradiance, $E_d(\lambda, z)$ and $E_u(\lambda, z)$, respectively (in W m$^{-2}$ nm$^{-1}$, where $z$ is depth in meters), were measured at 13 wavelengths with a vertical resolution of 0.08–0.16 m using an underwater spectroradiometer (SPMR, Satlantic Inc. Halifax, Canada), under clear sky (most cases) or homogenous overcast conditions. Downward irradiance was also simultaneously recorded in air [$E_d(\lambda, 0^+)$] using either the same instrument or a spectrally matched spectroradiometer (SMSR). Radiometers had been calibrated less than 3 months before each cruise by the instrument manufacturer. Platform (ship and helicopter) shadow was avoided and, in the specific case of the helicopter, instruments were deployed from an altitude high enough to avoid perturbation at sea surface created by the rotor air flux. The data with an instrument tilt >5° were removed such that the in-water vertical profiles start at a depth of approximately 2 m when the radiometers were deployed using a winch or in the free-falling mode from a ship, and at a depth of approximately 0.2 m when deployed from a helicopter using a winch. The $E_u(\lambda, z)$ data were corrected for instrument self-shading using the method described by *Mueller and Austin* [1995]. To estimate upward irradiance just below the surface [$E_u(\lambda, 0^-)$], the $E_u(\lambda, z)$ versus depth profiles were extrapolated up to surface by fitting the data to an exponential function. Downward irradiance just below surface [$E_d(\lambda, 0^-)$] was estimated by multiplying $E_d(\lambda, 0^+)$ by 0.94 to account for specular reflection (value in accordance with the range of the solar zenith angles in the COASTlOOC data set). The subsurface irradiance reflectance $R(\lambda)$ (dimensionless) just below the surface was calculated as the ratio $E_u(\lambda, 0^-)/E_d(\lambda, 0^-)$. The spectral values of $K_d(\lambda)$ were estimated by fitting an exponential function to the $E_d(\lambda, z)$ versus $z$ profiles from the depth where surface lens effects are qualitatively absent in $E_d(\lambda, z)$ down to the first attenuation depth where $E_d(\lambda, z) = 0.368\ E_d(\lambda, 0^-)$.

### 2.3. Additional In Situ Data Sets Used for Validation

[15] As one relationship in our $c(490)$ algorithm (between the scattering coefficient and the backscattering coefficient) is statistically derived using the COASTlOOC data set, we considered additional in situ data in order to validate inde-

pendently that algorithm. There are only a few data sets that include a wave band at 709 nm for reflectance and simultaneous measurements of IOPs, thus severely restricting the possibility for validation. We considered four data sets, briefly described below, that included simultaneous ac-9 measurements and irradiance or radiance reflectance above or below the water surface.

[16] The first data set was obtained during the CASES campaign which took place in the southeastern Beaufort Sea during the summer of 2004 [*Bélanger et al.*, 2006]. The bio-optical measurements of this data set used here are $c(490)$, and the above-surface or below-surface remote-sensing reflectance $R_{rs}(\lambda)$, or $r_{rs}(\lambda)$, (both in $sr^{-1}$), at 490 and 700 nm. The remote-sensing reflectances were either measured from above the sea surface using a hyperspectral radiometer (Analytical Spectral Device; 14 spectra) or in-water using SPMR/SMSR radiometers deployed from the ship deck (34 spectra) (for details on the methods, see the work by S. Bélanger et al., Improved quantification of Chromophoric Dissolved Organic Matter photooxidation in coastal waters using satellite-derived inherent optical properties, submitted to *Journal of Geophysical Research*, 2007). The second data set was obtained in Lunenburg Bay, Nova Scotia, Canada, during the summer of 2003 [see *Huot et al.*, 2007]. The measurements of interest for this study are $c(490)$, the hyperspectral downwelling irradiance above the surface $E_d(\lambda, 0^+)$, the hyperspectral upwelling radiance $L_u(\lambda, -0.65)$ measured at 0.65 m below the surface and $E_d(490, -2.58)$ measured at 2.58 m below the surface. The latter three were obtained from instruments attached to a single mooring. To obtain the upwelling radiance just below the surface, we propagated the measurements at 0.65 m, using $K_d$ as a proxy for $K_{Lu}$. At 490 nm, $K_d$ was calculated from the measurements of the surface sensor and the sensor located at 2.58 m, while at 709 nm, $K_w(709)$ was used as proposed by *Morel and Maritorena* [2001]. The third data set consists of data collected during the RSFlux campaigns in autumn 2005 over the Elbe and Gironde estuaries (D. Doxaran, personal communication, 2006). The beam attenuation coefficient $c$ was measured at 440 and 555 nm, and we used a linear interpolation between these bands to obtain $c(490)$. The above-surface remote-sensing reflectance $R_{rs}$ spectra were measured hyperspectrally and converted for the present study into $r_{rs}$, using the model of *Lee et al.* [2005a]. For the campaigns CASES, Lunenburg Bay and RSFlux, to convert the below-surface remote-sensing reflectances $r_{rs}$ into the irradiance reflectances $R(0^-)$, which are the inputs to the algorithm, ($R = r_{rs}\ Q$), we assumed a constant $E_u(0^-)/L_u(0^-)$ ratio (the $Q$ factor) of 4, a representative value for case 2 waters according to the calculations of *Loisel and Morel* [2001]. The fourth data set was collected during the Productivity of Oceanic Pelagic Systems (PROSOPE) cruise which sampled the Moroccan upwelling zone and the Mediterranean Sea [*Claustre et al.*, 2002]. The measurements of $c(490)$ and the irradiance reflectances under the sea surface were used in the present study. At given stations, we averaged replicate samples.

[17] These four data sets contain very diversified water types, NAP-dominated waters for the CASES campaign, CDOM-dominated waters in Lunenburg Bay, waters highly loaded with mineral particles for the RSFlux campaigns, and case 1 waters for the PROSOPE campaign. They were also obtained with diverse methodologies (above or below sea surface, radiance or irradiance reflectance) and by different investigators.

## 3. Description of the Algorithms

[18] Each step of the algorithm development is detailed in this section. The validity of the assumptions used is discussed with reference to the literature and to our data sets in section 4. First, an algorithm for retrieving $a(490)$ and $b_b(490)$ using irradiance reflectance in two bands (490 and 709 nm) is developed. Then, algorithms for retrieving $K_d(490)$, $c(490)$, and vertical visibility, from the estimated $a(490)$ and $b_b(490)$, are presented.

### 3.1. The Retrieval of $a$ and $b_b$

[19] The spectral irradiance reflectance just below the sea surface can be expressed as:

$$R(\boldsymbol{\lambda}) = \frac{E_u(\boldsymbol{\lambda})}{E_d(\boldsymbol{\lambda})} = f(\boldsymbol{\lambda})\frac{b_b(\boldsymbol{\lambda})}{a(\boldsymbol{\lambda})} \tag{1}$$

where

$$b_b(\boldsymbol{\lambda}) = b_{bw}(\boldsymbol{\lambda}) + b_{bp}(\boldsymbol{\lambda}), \tag{2}$$

$$a(\boldsymbol{\lambda}) = a_w(\boldsymbol{\lambda}) + [a(\boldsymbol{\lambda}) - a_w(\boldsymbol{\lambda})], \tag{3}$$

$\boldsymbol{f}(\lambda)$ is a factor that varies between approximately 0.2 and 0.45 mostly depending on IOPs and solar zenith angle [*Loisel and Morel*, 2001], $b_{bw}(\lambda)$ and $b_{bp}(\lambda)$ are the backscattering coefficients of pure seawater and marine particles, respectively, and $a_w(\lambda)$ is the absorption coefficient of pure seawater. The latter relationship and the following assumptions are assessed later in the paper for clarity.

[20] On the basis of the study of *Babin and Stramski* [2002], it is assumed that:

$$a(709) \equiv a_w(709) \tag{4}$$

[21] *Babin et al.* [2003b] and *Barnard et al.* [1998] observed small spectral variations in the scattering coefficient of marine particles, $b_p(\lambda)$, in the visible wave bands. In the Barnard et al. data set, the $b_p(555)/b_p(676)$ ratio averages 1.13. Given that the backscattering-to-scattering ratio for marine particles, $\tilde{b}_{bp}(\lambda)$, shows very weak spectral variations between 490 and 709 nm [*Twardowski et al.*, 2001], it is therefore assumed that:

$$b_{bp}(490) \equiv B_{490-709} b_{bp}(709) \tag{5}$$

with $B_{490-709}$, being constant.

[22] Using equations (1), (2), (3), (4), and (5), the estimated values of the backscattering and absorption coefficients at 490 nm, $\hat{b}_b(490)$ and $\hat{a}(490)$, can be expressed as:

$$\hat{b}_b(490) = B_{490-709}\left[\frac{a_w(709)}{f(709)}R(709) - b_{bw}(709)\right] + b_{bw}(490) \tag{6}$$

$$\hat{a}(490) = \frac{f(490)\hat{b}_b(490)}{R(490)} \tag{7}$$

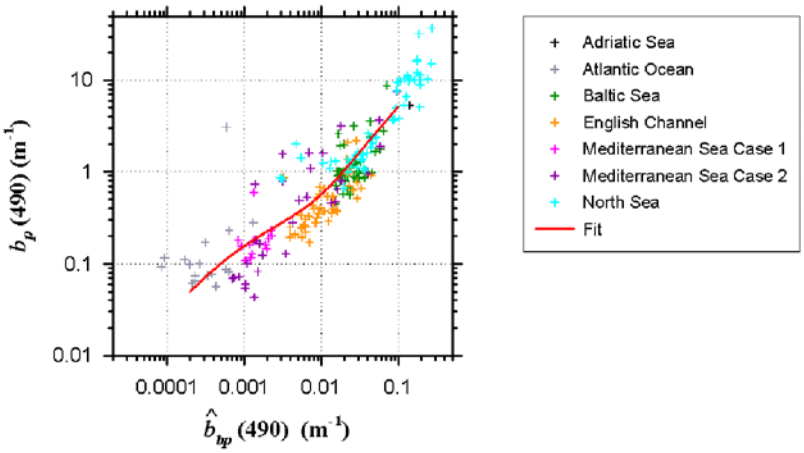


**Figure 1.** Relationship between the measured particle scattering coefficient at 490 nm $b_p(490)$ and the estimated particle backscattering coefficient at 490 nm $\hat{b}_{bp}(490)$ for the in situ COASTlOOC data set. The estimates of $\hat{b}_{bp}(490)$ were obtained with the nominal version of the algorithms using two reflectance bands as inputs, $R(490)$ and $R(709)$.

[23] Thus, if $a_w(709)$, $b_{bw}(490)$, $b_{bw}(709)$, $f(490)$, and $f(709)$ are known, the values of $a(490)$ and $b_b(490)$ can be obtained from measurements of $R(490)$ and $R(709)$. Here we used for $a_w(709)$ the value interpolated from the $a_w(\lambda)$ spectrum measured by *Pope and Fry* [1997], and for $b_{bw}(490)$ and $b_{bw}(709)$, we used the values interpolated from the spectrum of $b_w$ measured by *Morel* [1974], divided by 2 to account for the backscattering-to-scattering ratio of molecular scattering. For the additional campaigns (CASES, Lunenburg Bay, RSFlux and PROSOPE), we took into account the salinity and its influence on the water scattering and backscattering coefficients as in the work of *Boss and Pegau* [2001]. The values of $f(490)$ and $f(709)$ are assumed constant and are obtained from the literature (see section 4).

### 3.2. Algorithm to Estimate $K_d(490)$

[24] *Lee et al.* [2005b] recently published an extensive study on the relationship between the diffuse attenuation coefficient for downwelling irradiance determined between the depths of $E_d(0^-)$ and 10% of $E_d(0^-)$, $\bar{K}_d$ ($E_{10}$%), and $a$, $b_b$, and the solar zenith angle. We recall here their equation (11) that we use to estimate $K_d(490)$ from our estimates $\hat{b}_b(490)$ and $\hat{a}(490)$ and from the known solar zenith angle $\theta_s$ (deg) above the water:

$$\hat{K}_d(490) = (1 + 0.005\theta_s)\hat{a}(490) + 4.18\left(1 - 0.52e^{-10.8\hat{a}(490)}\right)\hat{b}_b(490) \quad (8)$$

Under cloudy conditions, $\theta_s$ is given the value of 45° as in the work of *Lee et al.* [2005a].

### 3.3. Algorithm to Estimate $c(490)$

[25] The backscattering-to-scattering ratio for particles is defined as: $\tilde{b}_{bp}(\lambda) = \frac{b_{bp}(\lambda)}{b_p(\lambda)}$.

[26] To realistically account for the variations of $\tilde{b}_{bp}(490)$ in the algorithm to retrieve $\boldsymbol{c}(490)$, we analyzed the relationship between $b_p(490)$ and $\hat{b}_{bp}(490)$ in the COASTlOOC data set. Figure 1 shows the scatterplot of $b(490) - b_w(490)$ [$= b_p(490)$] measured in situ, as a function of $b_b(490) - b_{bw}(490)$ [$= \hat{b}_{bp}(490)$], estimated from the reflectances at 490 and 709 nm [(equation (6)] for the COASTlOOC data set. The following expression between $\hat{b}_{bp}(490)$ and $b_p(490)$ is obtained empirically with the COASTlOOC data set:

$$\hat{b}_p(490) = \frac{\hat{b}_{bp}(490)}{-0.0310 + 0.0503\tanh\left(\frac{\hat{b}_{bp}(490) + 0.00686}{0.00820}\right)} \quad (9)$$

[27] Because $c = a + b$, the attenuation coefficient at 490 nm can be expressed as:

$$\hat{c}(490) = \hat{a}(490) + \hat{b}_p(490) + b_w(490) \quad (10)$$

[28] Thus, in addition to the IOPs of pure water, $f(490)$, $f(709)$, and $B_{490-709}$, the estimation of $c(490)$ from $R(490)$ and $R(709)$ requires the empirical relationship obtained in equation (9).

### 3.4. Algorithm to Estimate Vertical Visibility

[29] The Secchi depth is a measurement of vertical visibility. Its determination is dependent on observation conditions, including sun elevation, cloud cover, and sea state. IOPs and AOPs are certainly more robust indices of visibility, but the Secchi depth is easy to measure and to interpret by a wide range of users. Moreover, there exist historical records of the Secchi depth that go back to the beginning of the twentieth century.

[30] According to *Tyler* [1968] and *Preisendorfer* [1986], the Secchi depth ($Z_{SD}$, m) can be expressed by an equation that describes the photopic contrast reduction for a vertical path of sight in a homogeneous medium:

$$Z_{SD} = \frac{\ln\left(\frac{C_0}{C_{min}}\right)}{K_d(v) + c(v)}, \quad (12)$$

where $c(v)$ is the visual photopic beam attenuation coefficient, $K_d(v)$ is the visual photopic vertical diffuse

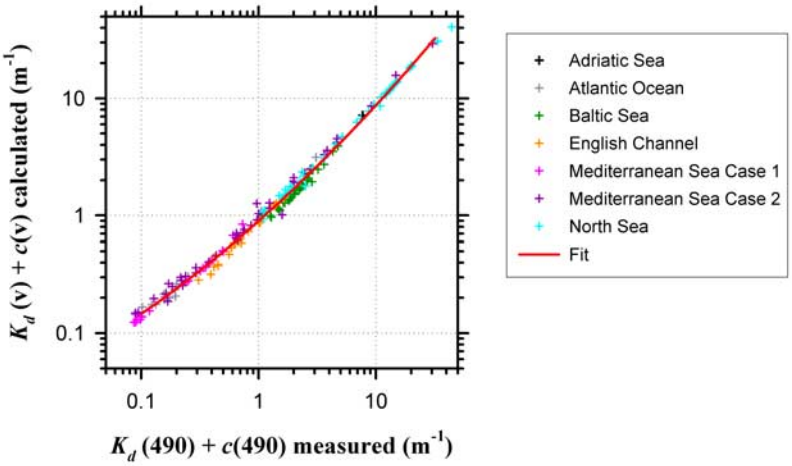


**Figure 2.** Relationship between the sum of the visual attenuation coefficient and the visual beam attenuation coefficient $K_d(v) + c(v)$ versus the measured vertical attenuation coefficient and the beam attenuation coefficient at 490 nm $K_d(490) + c(490)$ for the in situ COASTlOOC data set. The fit is quadratic polynomial.

attenuation coefficient of the medium (here v stands for visual), $C_0$ is the inherent contrast between the disk and background water, and $C_{min}$ is the minimum apparent contrast perceivable by the human eye. The photopic properties are the properties of the medium, depth-averaged, and spectrally weighted by the ambient light field and the photopic function, typical of the human sight in daylight conditions.

[31] The sensitivity of the human eye is described by the photopic function [e.g. *Mobley*, 1994]. Assuming that $K_d(490) + c(490)$ is strongly related to $K_d(v) + c(v)$ with a polynomial function $P$ (see Figure 2), the Secchi depth can be estimated using the following expression:

$$\hat{Z}_{SD} = \frac{\ln\left(\frac{C_0}{C_{min}}\right)}{P\left(\hat{K}_d(490) + \hat{c}(490)\right)} \tag{13}$$

According to *Preisendorfer* [1986], $\ln\left(\frac{C_0}{C_{min}}\right)$ can vary, with the submerged disk reflectance, the reflectance of the background and $C_{min}$, between 5 and 10. Since the COASTlOOC data set does not include Secchi depths, we use $\frac{1}{\hat{K}_d(490)+\hat{c}(490)}$ to evaluate the algorithm.

## 4. Assessment of the Algorithms Assumptions

[32] In this section, we assess the assumptions made in the development of our algorithms through a review of the recent literature and with reference to our data sets.

### 4.1. Relationship Between Reflectance and IOPs

[33] Equation (1) provides the relationship between reflectance and IOPs. *Gordon et al.* [1975] and *Morel and Prieur* [1977] found $f$ equal to 0.33 for a flat sea surface and the sun at zenith. *Morel and Gentili* [1996] and *Loisel and Morel* [2001] have shown that $f$ covers a variation range between approximately 0.25 and 0.45 with varying sun zenith angle and IOPs. The following expression, introduced by *Gordon et al.* [1975], is another equation relating reflectance to IOPs:

$$R(\lambda) = f'(\lambda)\frac{b_b(\lambda)}{a(\lambda) + b_b(\lambda)} \tag{14}$$

[34] Equation (14) is generally thought to be more appropriate for waters where scattering is high relative to absorption. Indeed, in equation (1), should very high values of backscattering be observed, the value of $f$ might become very small, while $f'$ should be more stable [*Loisel and Morel*, 2001]. Nevertheless, such conditions were not observed in the COASTlOOC data set, the $b/a$ ratio was always below 30 at both 490 and 709 nm. Since the COASTlOOC data set can be considered fairly comprehensive, apart from exceptionally turbid waters, most naturally occurring $f$ values are present in this data set. Under such conditions, according to the calculations of *Loisel and Morel* [2001], $f$ and $f'$ vary between 0.27 and 0.47, and 0.27 and 0.62, respectively, for sun zenith angles going from 0° to 60°. The use of equation (1) in this study is therefore expected to be more robust.

[35] The numerical values for $f(490)$ and $f(709)$ were obtained using the results of *Loisel and Morel* [2001]. Their Tables 3 and 4 are used to compute an average for all solar angles lower than 60° and two types of water (yellow substance and sediment dominated) described in their analysis. The values of $f(490)$ and $f(709)$ in the algorithms are thus set to 0.335.

### 4.2. Absorption in the Near-IR

[36] The absorption coefficient of pure seawater is high in the near-infrared while, above 750 nm, phytoplankton and CDOM absorption is negligible [*Bricaud and Stramski*, 1990; *Bricaud et al.*, 1981]. According to *Babin and Stramski* [2002, 2004], near-IR absorption by nonalgal particles is also negligible above 750 nm for many types of marine particles, but *Tassan and Ferrari* [2003] found

that some types of mineral particles, including those originating from river beds likely influenced by anthropogenic activity, do absorb light significantly in the near-IR.

[37] At 709 nm, it can be expected that phytoplankton, CDOM, and nonalgal particles show some absorption. In the COASTlOOC samples, the maximum values of the absorption coefficients determined separately for these three components, as described by *Babin et al.* [2003a], were 0.037, 0.011, and 0.035 $m^{-1}$, respectively, which is small compared with the value of 0.799 $m^{-1}$ for pure water reported by *Pope and Fry* [1997]. These maxima did not occur at the same station. For the 317 available stations with the absorption coefficient spectrophotometrically measured independently for phytoplankton, nonalgal particles, and CDOM, the ratio $[a(709) - a_w(709)]/a_w(709)$ averaged 1.35% (SD = 1.459) with an extreme value of 8.51%. Note, however, that the validity of this analysis depends on the protocol followed for the absorption measurements, where $a(750) - a_w(750)$ was assumed to equal 0 [*Babin et al.*, 2003b]. It is nevertheless reasonable to assume that absorption at 709 nm is largely dominated by water. *Sullivan et al.* [2006] measured the effect of a temperature change on the water absorption coefficient. Using their results in the NIR, the changes in temperature have a very slight impact on the estimation of $\hat{a}$ and $\hat{b}_b$. The relative error between the quantities $\hat{a}$ and $\hat{b}_b$ estimated with $a_w$ measured by *Pope and Fry* [1997] and the quantities estimated with a ±10°C variation is on average ±0.025 (SD = 0.0057) for the COASTlOOC data set. This can be considered as negligible in the context of our algorithms, but this effect could nevertheless be accounted for with simultaneous measurements of sea surface temperature or climatological maps.

### 4.3. Scattering Properties of Particles

[38] In previous attempts to model marine reflectance, the particle scattering coefficient, $b_p(\lambda)$, was assumed based on theoretical considerations to vary as a function of $\lambda^{-n}$ with $n$ varying between 0 and 2 [e.g. *Sathyendranath et al.*, 1989]. The observations of *Barnard et al.* [1998] and *Babin et al.* [2003a] both indicate that the $b_p(\lambda)$ spectrum is poorly represented by a $\lambda^{-n}$ function in the visible range. In typical case 1 surface waters, the $b_p(\lambda)$ spectrum is characterized by a general increase toward shorter wavelengths and significant troughs in the spectral ranges of major phytoplankton pigment absorption bands. In typical case 2 waters, the $b_p(\lambda)$ spectrum generally shows a slighter increase toward shorter wavelengths and is less featured. In 239 samples collected by *Babin et al.* [2003a] around Europe in case 1 and case 2 waters, the mean spectrum of the scattering coefficient deviated by at most ±5% from a flat spectrum with a null slope. On the basis of *Barnard et al.*'s [1998] results at 555 and 676 nm, we use for the ratio of $B_{490-709} = b_p(490)/b_p(709)$, a value of 1.13 [equation (5)] as representative of natural waters, especially coastal ones.

### 4.4. Backscattering Efficiency of Particles

[39] The backscattering efficiency of particles, $\tilde{b}_{bp}$, is known to vary as a function of the size and refractive index of the particles (reviewed by *Stramski et al.* [2004]). In the recent observations made by *Boss et al.* [2004] in coastal waters, $\tilde{b}_{bp}$ varied between 0.005 and 0.035. Most values lay within 0.005–0.015, while the higher values were observed near the bottom. In case 1 waters, *Morel et al.* [2007] observed variations of $\tilde{b}_{bp}$ between 0.006 and 0.014 and found the $\tilde{b}_{bp}(\lambda)$ spectrum to be essentially flat. In the COASTlOOC data set, more mineral particles were found in coastal waters [*Babin et al.*, 2003a], and higher $\tilde{b}_{bp}$ (490) can be expected for such particles because of their higher refractive index [*Twardowski et al.*, 2001; *Sullivan et al.*, 2005]. The value of $\tilde{b}_{bp}(490)$ is also determined by the size distribution of particles, but the first determinant in the COASTlOOC data set is the refractive index [*Babin et al.*, 2003a]. Whether or not such a coastal versus open ocean trend (decreasing refractive index) depicted by equation (9) is representative at global scale remains to be documented. However, it is likely that waters with a high $b_p(490)$ resulting from an algal bloom can be expected to have a low $\tilde{b}_{bp}(490)$ and, therefore, not to follow the trend depicted by equation (9). It is important to stress that equation (9) is only valid for the $b_{bp}$ retrieved by our algorithm. It may well reflect, and correct for, a bias of that algorithm. However, in any case, the use of equation (9) does lead to better estimates of $c(490)$ than when using a constant $b_{bp}(490)/b_p(490)$ ratio. Since equation (9) was obtained using the COASTlOOC data set, we validate our $c(490)$ algorithm also using independent in situ data sets, CASES, Lunenburg Bay, RSFlux, and PROSOPE.

### 4.5. Relationship Between $K_d(490) + c(490)$ and $K_d(v) + c(v)$

[40] The $K_d(v)$ and $c(v)$ coefficients were calculated for the COASTlOOC data set, following *Preisendorfer* [1986], using the photopic function tabulated in *Mobley* [1994] and the spectral measurements of $K_d(\lambda)$, $c(\lambda)$, $E_u(\lambda)$, and $E_d(\lambda)$. Figure 2 displays the relationship between $K_d(490) + c(490)$ and $K_d(v) + c(v)$. Above 0.3 $m^{-1}$, the relationship is very tight and close to linear. Below 0.3 $m^{-1}$, $K_d(v) + c(v)$ is systematically higher than $K_d(490) + c(490)$. This is because the photopic function peaks around 550 nm and thus weighs $K_d(\lambda) + c(\lambda)$ more strongly around that wavelength. Above 0.3 $m^{-1}$, $K_d(490) + c(490)$ is close to $K_d(550) + c(550)$, thence the tight relationship with $K_d(v) + c(v)$. Below 0.3 $m^{-1}$, $K_d(490) + c(490)$ is systematically lower than $K_d(550) + c(550)$, thence the bias observed in Figure 2 [see also *Zaneveld and Pegau*, 2003]. A second order polynomial can be fitted on this scatterplot, giving an $R^2$ greater than 0.99. The resulting equation is $P(x) = 0.0989x^2 + 0.8879x - 0.0467$. Overall, $[P(\hat{K}_d(490) + \hat{c}(490))]^{-1}$ is a good index of vertical visibility or water transparency measured using the Secchi depth, $Z_{SD}$.

[41] Because the sensitivity of the human eye peaks at 555 nm [e.g. *Mobley*, 1994], it may seem more appropriate to use $K_d(\lambda) + c(\lambda)$ with $\lambda$ close to 555 nm to estimate visibility. However, this wavelength corresponds to a trough in the absorption of phytoplankton, and the absorption of NAP and CDOM is lower at 555 nm than at shorter wavelengths. In addition, the absorption of pure seawater is larger at 555 nm than at shorter wavelengths. These two effects lead to a reduced range of variations in $K_d(555) + c(555)$ compared with $K_d(490) + c(490)$, and possibly a larger relative error. As a result, $K_d(555) + c(555)$ is less sensitive to changes in seawater color. Note that the changes in seawater color as perceived by the human eye (for example, clear versus phytoplankton-rich waters) are mostly

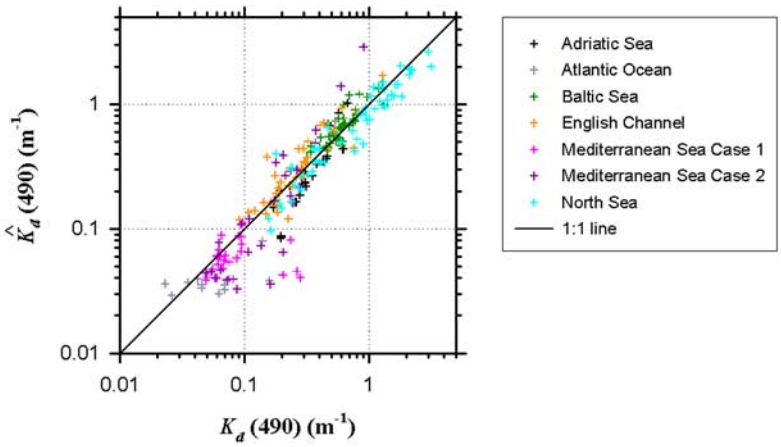


**Figure 3.** Relationship between the estimated vertical diffuse attenuation coefficient $\hat{K}_d(490)$ and the measured $K_d(490)$ for the in situ COASTlOOC data set. The estimates of $\hat{K}_d(490)$ were obtained with the nominal version of the algorithms using two reflectance bands as inputs, $R(490)$ and $R(709)$, and the determination coefficient $R^2$ is 0.88.

driven by changes in the optical properties of the blue range of the spectrum, where variations in AOPs are largest. The latter arguments and some quantitative verifications led us to adopt $K_d(490) + c(490)$ instead of $K_d(555) + c(555)$ to estimate visibility.

## 5. Results and Discussion

[42] In this section, we test the $K_d(490)$ and $c(490)$ algorithms using the COASTlOOC, IOCCG, and additional data sets. First, the parameters used in the algorithms, $f(490)$, $f(709)$, and $B_{490-709}$, are maintained constant, which constitutes the nominal version of the algorithm. Second, to test the robustness of the algorithms to variations in $f(490)$, $f(709)$ and $B_{490-709}$, we conduct a sensitivity study using the IOCCG data set. Finally, the algorithm to retrieve $c(490)$, partly relying on the COASTlOOC data set, is tested with the in situ data sets, CASES, Lunenburg Bay, RSFlux, and PROSOPE.

### 5.1. Algorithm Validation Using the COASTlOOC Data Set

[43] In this section, we use the COASTlOOC data set that covers several different open ocean and coastal environments to complete the first validation step. The comparisons between retrieved $\hat{K}_d(490)$, $\hat{c}$ (490), and $[\hat{K}_d(490) + \hat{c}\ (490)]^{-1}$, and the measured $K_d(490)$, $c(490)$, and resulting $[K_d(490) + c(490)]^{-1}$ are shown in Figures 3–5.

[44] The physical quantities considered here span over more than two orders of magnitude. The measurements ($K_d$ or $c$) as well as the algorithm outputs ($K_d$ or $c$ estimated with the measured reflectances $R$) are affected by measurement errors. For these reasons, a Type II linear regression has to be considered in log space. The error associated with the

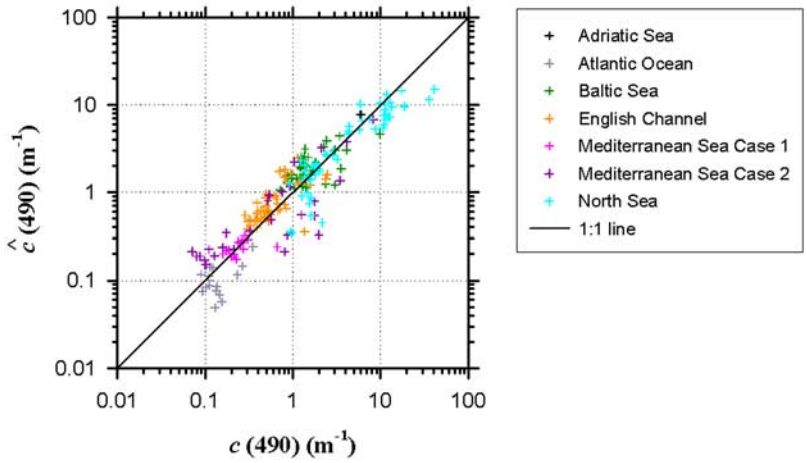


**Figure 4.** Relationship between the estimated beam attenuation coefficient $\hat{c}(490)$ and the measured $c(490)$ for the in situ COASTlOOC data set. The estimates of $\hat{c}(490)$ were obtained with the nominal version of the algorithms using two reflectance bands as inputs, $R(490)$ and $R(709)$, and the determination coefficient $R^2$ is 0.86.

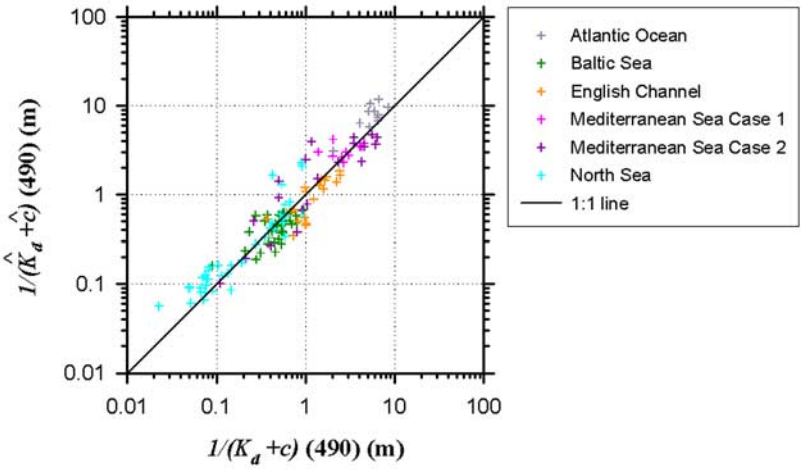


**Figure 5.** Relationship between the estimated inverse of the sum of the vertical diffuse attenuation coefficient and the beam attenuation coefficient $[\hat{K}_d(490) + \hat{c}(490)]^{-1}$ and the measured $[K_d(490) + c(490)]^{-1}$ for the in situ COASTlOOC data set. The estimates of $[\hat{K}_d(490) + \hat{c}(490)]^{-1}$ were obtained with the nominal version of the algorithms using two reflectance bands as inputs, $R(490)$ and $R(709)$, and the determination coefficient $R^2$ is 0.90.

retrievals by our algorithm was quantified using the 95% "geometric" confidence interval around the 1:1 line of the relationships between estimated and measured values. Because the residuals had to be log transformed to get closer to normality and homogeneity, the 95% confidence interval was calculated as:

$$95\%\ \text{confidence interval} = 10^{1.96\text{SD}_{\log 10}}$$

where $\text{SD}_{\log 10}$ is the arithmetic standard deviation calculated on log transformed residuals. This error metric is to be applied as a factor for both the retrieval of $K_d(490)$ and $c(490)$.

[45] Tables 2–4 summarize for each comparison between retrieved and simulated or measured values the following statistics: number of samples, determination coefficient, intercept and slope of the Type II regression, and 95% geometric confidence interval, for $K_d$, $c$ and $[K_d(490) + c(490)]^{-1}$, respectively.

[46] Figure 3 shows the comparison between $\hat{K}_d(490)$, retrieved using equations (6), (7), and (8), and $K_d(490)$ from the COASTlOOC data set. There is some scatter, but the data points are rather well distributed around the 1:1 line. The determination coefficient on log-transformed data is high at 0.88, and the estimates are 95% reliable within a factor of 2.21. The slope (1.09) and the intercept (0.012) are close to 1 and 0, respectively. Given that $K_d(490)$ varies over more than two orders of magnitude, this result can certainly be considered as satisfactory.

[47] Figure 4 shows the comparison between the $\hat{c}(490)$ retrieved using equations (6), (7), (9), and (10), and the measured $c(490)$. The determination coefficient $r^2$ is 0.86 on log-transformed data, and the data are rather well distributed around the 1:1 line. The slope and intercept of the $\hat{c}(490)$ versus $c(490)$ regression, 0.94 and −0.0039, respectively, are close to 1 and 0 (Table 3). The estimates are reliable within a factor of 2.71.

[48] Figure 5 shows the comparison between $[\hat{K}_d(490) + \hat{c}(490)]^{-1}$ and $[K_d(490) + c(490)]^{-1}$ for the COASTlOOC data set, where $[\hat{K}_d(490) + \hat{c}(490)]^{-1}$ was retrieved using equations (6), (7), (8), and (9). The determination coefficient $r^2$ is 0.90 on log-transformed data. The Type II regression gives a slope of 0.98 and an intercept of 0.0175. We consider that the algorithm gives a very good retrieval of $[\hat{K}_d(490) + \hat{c}(490)]^{-1}$.

[49] The algorithm to retrieve $K_d$ gives very good results for the COASTlOOC data. As the entire development of the algorithm is realized without reference to COASTlOOC, it

**Table 2.** Statistics for the Algorithm Described in the Text to Retrieve $K_d(490)$ for All Data Sets[a]

| Data Set and Algorithm | $f$ | $B_{490-709}$ | $N$ | $R^2$ | Slope | Intercept | 95% Confidence Interval |
|---|---|---|---|---|---|---|---|
| COASTlOOC, $K_d(490)$, | $f(490) = 0.335$ $f(709) = 0.335$ | 1.13 | 229 | 0.88 | 1.09 | 0.0120 | 2.21 |
| IOCCG, $K_d(490)$, | $f(490) = 0.335$ $f(709) = 0.335$ | 1.13 | 1000 | 0.99 | 1.06 | 0.0362 | 1.49 |
| IOCCG, $K_d(490)$, | "Station"-calculated | 1.13 | 1000 | 0.99 | 1.04 | 0.0291 | 1.38 |
| IOCCG, $K_d(490)$, | $f(490) = 0.335$ $f(709) = 0.335$ | "Station"-calculated | 1000 | 0.99 | 0.99 | 0.0139 | 1.15 |
| IOCCG, $K_d(490)$, | "Station"-calculated | "Station"-calculated | 1000 | 0.99 | 0.98 | 0.0076 | 1.14 |
| COASTlOOC, $K_d(490)$ [*Lee et al.*, 2005b] | | | 229 | 0.87 | 0.99 | −0.0071 | 2.06 |

[a]The nominal algorithm uses as input the irradiance reflectances at 490 and 709 nm and constant $f$ and $B_{490-709}$ values (see text). The tests of robustness are made with $f$ or $B_{490-709}$ variable for each "station." The regression results are of Type II on log-transformed data. The calculation of the 95% confidence interval (to be applied as a factor) is described in section 5.

**Table 3.** Statistics for the Algorithm Described in the Text to Retrieve $c(490)$ for All Data Sets[a]

| Data Set and Algorithm | $f$ | $B_{490-709}$ | $N$ | $R^2$ | Slope | Intercept | 95% Confidence Interval |
|---|---|---|---|---|---|---|---|
| COASTlOOC, $c(490)$, | $f(490) = 0.335$ $f(709) = 0.335$ | 1.13 | 202 | 0.86 | 0.94 | −0.0039 | 2.71 |
| IOCCG, $c$ (490), | $f(490) = 0.335$ $f(709) = 0.335$ | 1.13 | 1000 | 0.97 | 0.95 | −0.0100 | 1.54 |
| IOCCG, $c$ (490), | "Station"-calculated | 1.13 | 1000 | 0.98 | 0.91 | −0.0629 | 1.54 |
| IOCCG, $c$ (490), | $f(490) = 0.335$ $f(709) = 0.335$ | "Station"-calculated | 1000 | 0.97 | 0.85 | 0.0079 | 1.74 |
| IOCCG, $c$ (490), | "Station"-calculated | "Station"-calculated | 1000 | 0.98 | 0.80 | −0.0456 | 1.83 |
| CASES, Lunenburg Bay, RSFlux, and PROSOPE, $c$ (490) | $f(490) = 0.335$ $f(709) = 0.335$ | 1.13 | 95 | 0.95 | 1.12 | −0.02 | 2.91 |

[a]The nominal algorithm uses as input the irradiance reflectances at 490 and 709 nm and $f$ and $B_{490-709}$ values are constant. The tests of robustness are made with $f$ or $B_{490-709}$ variable for each "station." The regression results are of Type II on log-transformed data. The calculation of the 95% confidence interval (to be applied as a factor) is described in section 5.

means that this algorithm is validated on an independent in situ data set. The development of the algorithm to retrieve $c$ depends partly on the COASTlOOC data set, through the relationship between the particle backscattering and scattering coefficients [equation (9)]. The excellent results obtained on the COASTlOOC data are therefore not independent, and we henceforth validate this algorithm with independent in situ data sets (see section 5.4 below).

### 5.2. Algorithm Validation Using the IOCCG Data Set

[50] The most significant differences between the assumptions of our algorithms and the input of the IOCCG radiative transfer simulations are (1) $a$-$a_w(709)$ in the IOCCG data set is not assumed to be null as in equation (4) but rather changes according to the randomly varying composition of seawater, (2) the ratio of $b_b$-$b_{bw}$ at 490 and 709 nm (and $b_b$-$b_{bw}$ at 490 and 560 nm) in the IOCCG data set is not assumed to be constant as in equation (5) but rather changes according to variable proportions of phytoplankton and other particles and their associated $n_1$ and $n_2$ parameters, which describe the spectral variations of the beam attenuation coefficient of phytoplankton and the scattering coefficient of nonalgal particles, respectively, and (3) different phase functions are applied for the different optically significant seawater components in the IOCCG data set (see section 2 and *Lee et al.* [2005b] for details). It is worth noting, however, that the variations of $b$ and $b/a$ in the IOCCG data set and in the COASTlOOC data set cover the same range.

[51] The comparisons between retrieved $\hat{K}_d(490)$, $\hat{c}(490)$, and $[\hat{K}_d(490) + \hat{c}(490)]^{-1}$, and the simulated $K_d(490)$, $c(490)$, and $[K_d(490) + c(490)]^{-1}$ are shown in Figures 6–8, for the entire IOCCG data set. As expected, the scatter is less important than with the in situ data because it includes less natural variability in all optical parameters and excludes experimental errors.

[52] The comparison between $\hat{K}_d(490)$, obtained with equations (6), (7), and (8), and $K_d(490)$ gives a determination coefficient $R^2$ of 0.99 on log-transformed data, for both sun zenith angles of 30° and 60° (Figure 6). The algorithm yields estimates reliable within a factor of 1.49 (times and divided). The slope of the regression between $\hat{K}_d(490)$ and $K_d(490)$ is close to 1 (1.06) and the intercept is small (0.036 $m^{-1}$). The bias (underestimation of low $K_d$ values and overestimation of high $K_d$ values) is partly due to the spectral dependency of the particle scattering coefficient. In our algorithm, we assume the backscattering spectrum to be almost flat [see equation (5)], whereas in the IOCCG data set, for low chlorophyll $a$ concentrations (i.e., low $K_d(490)$ values), the scattering spectrum is closer to a $\lambda^{-2}$ spectral dependency. Given the information on particle scattering currently available in the literature, it is not possible to determine what parameterization is most representative of the natural environment [see *Babin et al.*, 2003b; *Lee et al.*, 2005a and references therein].

[53] We obtained a high $R^2$ of 0.97, on log-transformed data, for the comparison between $\hat{c}(490)$ and $c(490)$, where $\hat{c}(490)$ is obtained with equations (6), (7), (9), and (10). When comparing $\hat{c}(490)$ with $c(490)$ (Figure 7), a clear bias is observed. The $c$ algorithm overestimates $c$ for very low and high values of $c(490)$, whereas it underestimates the intermediate values. This bias is mainly due to the parameterization of the relationship between the estimated $\tilde{b}_{bp}$ and $b_p$, established with the COASTlOOC data set. In natural environments, the relationship between the two

**Table 4.** Statistics for the Algorithm Described in the Text to Retrieve $[K_d(490) + c(490)]^{-1}$ for All Data Sets[a]

| Data Set and Algorithm | $f$ | $B_{490-709}$ | $N$ | $R^2$ | Slope | Intercept | 95% Confidence Interval |
|---|---|---|---|---|---|---|---|
| COASTlOOC, $[K_d + c]^{-1}$ | $f(490) = 0.335$ $f(709) = 0.335$ | 1.13 | 139 | 0.90 | 0.98 | 0.0175 | 2.31 |
| IOCCG $[K_d + c]^{-1}$ | $f(490) = 0.335$ $f(709) = 0.335$ | 1.13 | 1000 | 0.98 | 0.98 | 0.0075 | 1.43 |
| IOCCG $[K_d + c]^{-1}$ | "Station"-calculated | 1.13 | 1000 | 0.99 | 0.93 | 0.0451 | 1.39 |
| IOCCG $[K_d + c]^{-1}$ | $f(490) = 0.335$ $f(709) = 0.335$ | "Station"-calculated | 1000 | 0.98 | 0.88 | −0.0199 | 1.56 |
| IOCCG $[K_d + c]^{-1}$ | "Station"-calculated | "Station"-calculated | 1000 | 0.99 | 0.83 | 0.0182 | 1.63 |

[a]The nominal algorithm uses as input the irradiance reflectances at 490 and 709 nm and $f$ and $B_{490-709}$ values are constant. The tests of robustness are made with $f$ or $B_{490-709}$ variable for each "station." The regression results are of Type II on log-transformed data. The calculation of the 95% confidence interval (to be applied as a factor) is described in section 5.

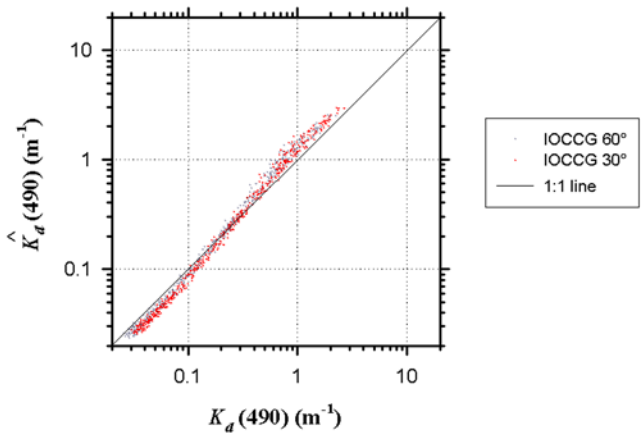


**Figure 6.** Relationship between the estimated vertical diffuse attenuation coefficient $\hat{K}_d(490)$ and the measured $K_d(490)$ for the synthetic IOCCG data set. The estimates of $\hat{K}_d(490)$ were obtained with the nominal version of the algorithms using two reflectance bands as inputs, $R(490)$ and $R(710)$, and the determination coefficient $R^2$ is 0.99.

quantities is expected to be more complex than in the IOCCG data set where 1% and 1.83% have been chosen for algal particles and nonalgal particles, respectively, and the proportion of these two component is varied randomly. We are thus more confident in a validation using an in situ data set than a simulated data set. The Type II regression provides a slope (0.95) and intercept (−0.01) close to 1 and 0, respectively, and the estimates are reliable within a factor of 1.54.

[54] On log-transformed data, the comparison between $[\hat{K}_d(490) + \hat{c}\ (490)]^{-1}$ and $[K_d(490) + c(490)]^{-1}$ gives a determination coefficient $R^2$ of 0.98 (Figure 8). The Type II regression gives a slope of 0.98 and an intercept of 0.0075. The estimates are reliable within a factor of 1.43.

[55] The algorithm to retrieve $K_d(490)$ gives excellent results. The algorithms to retrieve $c(490)$ and $[K_d(490) + c(490)]^{-1}$ show some biases on the simulated data set because of the parameterization chosen for the input IOPs, which is more artificial than the natural relationship, as obtained on the COASTlOOC data set. The simulated data set is nevertheless very useful to test the robustness of the algorithms, since all the parameters ($f$ and $B_{490-709}$) can be calculated for each "station."

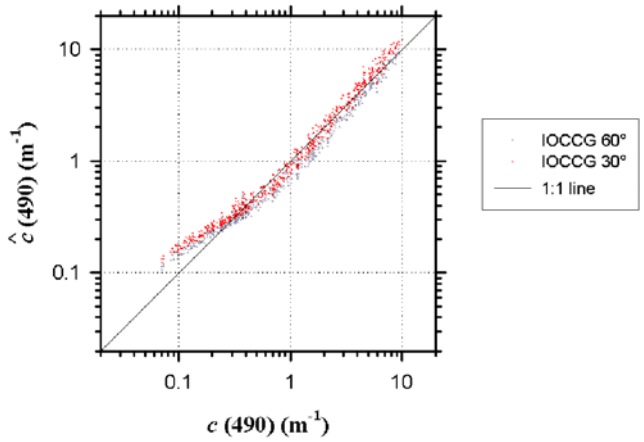


**Figure 7.** Relationship between the estimated beam attenuation coefficient $\hat{c}(490)$ and the measured $c(490)$ for the synthetic IOCCG data set. The estimates of $\hat{c}(490)$ were obtained with the nominal version of the algorithms using two reflectance bands as inputs, $R(490)$ and $R(709)$ and the determination coefficient $R^2$ is 0.97.

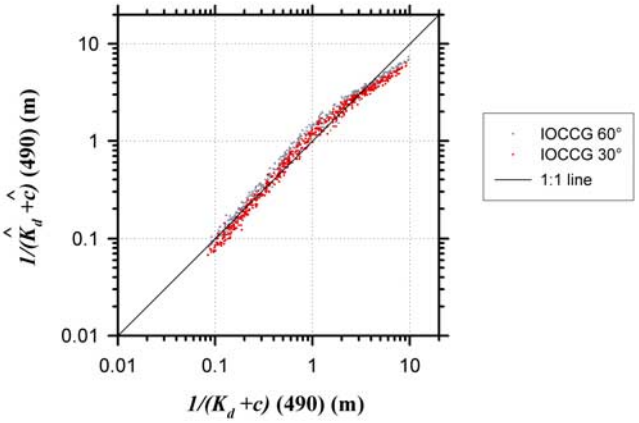


**Figure 8.** Relationship between the estimated inverse of the sum of the vertical diffuse attenuation coefficient and the beam attenuation coefficient $[\hat{K}_d(490) + \hat{c}\ (490)]^{-1}$ and the measured $[K_d(490) + c(490)]^{-1}$ for the synthetic IOCCG data set. The estimates of $[\hat{K}_d(490) + \hat{c}(490)]^{-1}$ were obtained with the nominal version of the algorithms using two reflectance bands as inputs, $R(490)$ and $R(709)$, and the determination coefficient $R^2$ is 0.90.

### 5.3. Robustness of the Algorithms Tested Using the IOCCG Data Set

[56] Part of the validity of the algorithms to estimate $K_d(490)$ and $c(490)$ relies on the values of $f(490)$, $f(709)$, and $B_{490-709}$. As the value of these parameters have been taken from the literature data, it is important to know whether the quality of the retrieval is sensitive to the chosen values. We conducted such a sensitivity study on the IOCCG data set because with this comprehensive simulated data set, it is possible to calculate the exact values of $f(490)$, $f(709)$, and $B_{490-709}$ for each simulated "station." We applied a modified version of the algorithm, each time with one of the parameters (either the $f$ values or $B_{490-709}$) taken equal at the "real" value for each "station," while the other parameter was held constant. The "exact" simulation is obtained when both $f$ and $B_{490-709}$ are calculated for each "station." The scatterplots in each case showed very similar features to the scatterplots obtained with the nominal algorithm (scatterplots not shown). The statistical results are presented in Tables 2, 3, and 4, and only minor differences can be seen between the proposed version of the algorithms and the ones for which one parameter is held constant. This leads to the conclusion that the algorithms are robust with the chosen parameterization.

[57] The validation conducted using the IOCCG data set confirms the robustness of the algorithms proposed here and reveals at the same time some biases. However, although the IOCCG data set is meant to be as realistic as possible, several of the assumptions made to design this artificial data set and to derive our algorithms remain poorly documented

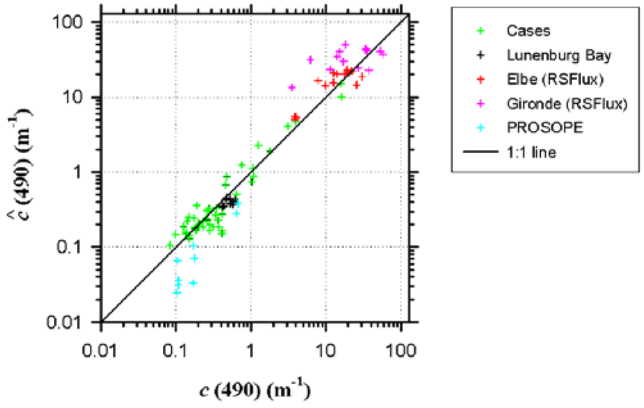


**Figure 9.** Relationship between the estimated beam attenuation coefficient $\hat{c}(490)$ and the measured $c(490)$ for the CASES, Lunenburg Bay, RSFlux, and PROSOPE data sets. Estimates of $\hat{c}(490)$ were obtained with the nominal version of the algorithms using two reflectance bands as inputs, $R(490)$ and $R(709)$, and the determination coefficient is 0.95.

in the current literature. This is particularly true for the assumptions made regarding the particle phase function [*Stramski et al.*, 2004]. Therefore we complete the validation of our algorithm using in situ data sets.

### 5.4. Validation Using Additional In Situ Data Sets

[58] Figure 9 shows the comparison between $\hat{c}(490)$ retrieved using equations (6), (7), (9), and (10), and the measured $c(490)$ for the four following campaigns: CASES, Lunenburg Bay, RSFlux, and PROSOPE. There is very good agreement among these campaigns over three orders of magnitude, although they occurred in very diverse water types. The determination coefficient $R^2$ is 0.95 on log-transformed data, and the data show features similar to the COASTlOOC data set. There is an overestimation for very turbid waters ($c(490) > 10$ m$^{-1}$) in estuarine waters, which may because of an overestimation of $\hat{b}_P$ (490) from $\hat{b}_{bP}$ (490). The estimates are reliable within a factor of 2.91, which is larger than for the COASTlOOC data set, but is still good, considering the variety of protocols and operators.

### 5.5. Comparisons With Published Algorithms

[59] A recent report of the *IOCCG* [2006] evaluates the progress to date in the retrieval of seawater IOPs using ocean color data. It presents a series of currently available algorithms and their performances when applied to synthetic and in situ IOCCG data sets. It is shown that the algorithm of *Lee et al.* [2002] for the retrieval of $a$ and $b_b$ performs among bests. In this section, we apply to the COASTlOOC data set the algorithm of *Lee et al.* [2005a] for the retrieval of $K_d(490)$. The latter is based on the $a$ and $b_b$ algorithms of *Lee et al.* [2002]. We then compare the performances of Lee et al.'s algorithm with those of our $K_d(490)$ algorithm.

[60] The first step in *Lee et al.*'s [2005a] $K_d(490)$ algorithm consists in using the remote sensing reflectance, $r_{rs}$ (defined as the ratio between upwelling radiance and downward irradiance) to retrieve the absorption coefficient and the backscattering coefficients [*Lee et al.*, 2002]. Two paths are proposed, the QAA-555 algorithm for most oceanic and coastal waters, which uses reflectance at three wavelengths (440, 490, and 555 nm) and three empirical relationships, and the QAA-640 algorithms for turbid waters, which uses reflectance at four wavelengths (440, 490, 555, and 640 nm) and two empirical relationships. In addition, if reflectance at 640 nm is not available (it is the case for sensors currently in flight), it is necessary to assume one more empirical relationship between the reflectances, which provides an estimate of the reflectance at 640 nm from the reflectances at 490, 555, and 667 nm. The combination of the two algorithms (optimized version) requires finally four wavelengths (440, 490, 555, and 667 nm in our data set) and five empirical relationships to retrieve $a(490)$ and $b_b(490)$. The second step consists in using the estimated $a(\lambda)$ and $b_b(\lambda)$ to retrieve $K_d(\lambda)$ [*Lee et al.*, 2005b]. To convert the subsurface irradiance reflectance $R(0^-)$, available in the COASTlOOC data set, to $r_{rs}$ ($R = r_{rs}\,Q$), we assumed a constant $E_u(0^-)/L_u(0^-)$ ratio (the so-called $Q$ factor) of 4, a representative value for case 2 waters according to the calculations of *Loisel and Morel* [2001]. When comparing the $\hat{K}_d(490)$ retrieved using the optimized QAA algorithm [*Lee et al.*, 2005b] with measured $K_d(490)$, we obtained a good agreement with an $R^2$ coefficient of 0.88 on log-transformed data (Figure 10). The estimates are reliable within a factor of 2.06, and the slope and intercept of the $\hat{K}_d$ (490) versus $K_d(490)$ regression are close to 1 and 0, respectively (Table 2). The performances of this algorithm are very similar to those of our algorithm. Lee et al.'s algorithm proves to be very robust when tested on the COASTlOOC data set which covers various types of water. It is worth noting that the assumption on $Q$ that we had to make for applying Lee et al.'s algorithm may have slightly degraded the results.

[61] While the performances of Lee at al.'s and our algorithms are very similar, their design are quite different. Lee et al.'s $K_d(490)$ algorithm is based on a number of empirical relationships obtained using various regional data sets. Those relationships are in part necessary because of the spectral domains that are used. At all wavelengths in the visible range, most optically significant constituents (pure seawater, phytoplankton, nonalgal particle, and CDOM) absorb and scatter light. No simplifying assumption can be made. While the empirical relationships used by *Lee et al.* [2005b] proved to be robust (*IOCCG* [2006] and this study), one disadvantage is that a fine tuning of their algorithm, for instance regionally, is difficult because it necessitates that these relationships be reestablished.

[62] On the contrary, the use of the near infrared wavelength 709 nm allows us to make simpler assumptions and to have recourse to a few parameters ($f$ and $B_{490-709}$) and one empirical relationship between the IOPs only. The parameterization and the empirical relationship proved to be robust, as assessed by the sensitivity study and the excellent retrieval using independent in situ data sets. However, the parameterization and the empirical relationship could be easily readjusted regionally from few in situ measurements or from published data.

## 6. Conclusion

[63] An alternative to complex hyperspectral and/or inverse modeling ocean color algorithms consists in using a combination of few wave bands judiciously selected in

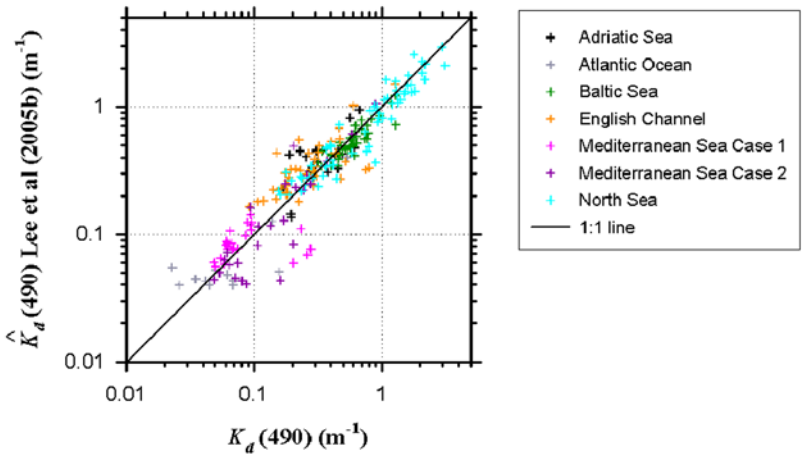


**Figure 10.** Relationship between the estimated vertical diffuse attenuation coefficient $\hat{K}_d$ (490) and the measured $K_d$(490) for the in situ COASTlOOC data set. Estimates of $\hat{K}_d$ (490) were obtained with the algorithms proposed by *Lee et al.* [2002, 2005a, 2005b]. The determination coefficient $R^2$ is 0.87.

spectral regions where variations in reflectance are well understood and can be reproduced using simple expressions and a few assumptions. The algorithms by *Ruddick et al.* [2001] for the retrieval of chlorophyll concentration in turbid waters and by *Simis et al.* [2005] for the retrieval of phycocyanin concentration in lakes are good examples of this alternative approach. This is also the path we chose with our algorithms. For the near-future operational ocean color missions such as NPOESS and Sentinel, such simple algorithms using few wave bands will be needed. The present study is a contribution to these needs. The algorithms presented here use reflectance at only two wavelengths. These wavelengths are available on the European Space Agency sensor MERIS and will be available on the Sentinel-3 sensors. One of these wavelength is 709 nm, located in the near infrared, and allows a simplifying assumption to be made concerning the absorption coefficient. This is original in the present study. The proposed algorithms are valid in both case 1 and case 2 waters and are largely insensitive to regional variability in optical properties. They consist in simple analytical expressions and involve few assumptions. An important aspect of these algorithms is that most parameters are described as measurable quantities (for example, the ratio between particle scattering coefficients at 490 and 709 nm) and/or can be derived from radiative transfer calculations (for example, the $f$ factor), which allows, if needed, a fine regional tuning of the algorithms using frequently measured optical properties. Thus establishing empirical coefficients regionally or measuring simultaneously the IOPs and reflectances is not necessary. In this study, we also proposed the first operational $c$ algorithm (the one by *Roesler and Boss* [2003] was designed for hyperspectral data).

[64] While the validation of our $K_d$(490) algorithm yielded satisfying results, our validation results for the $c$(490) calls for more research on the variability of the backscattering ratio. Although it has recently become more and more documented through simultaneous measurements of the particle scattering and particle backscattering coefficients [*Sullivan et al.*, 2005], it is still difficult to use this information to improve ocean color algorithms.

[65] Another issue with remote-sensing data is the availability and quality of the water-leaving reflectances at 709 nm retrieved by satellite-borne sensors. MERIS is currently the only sensor with this wavelength available. The NIR wavelengths also suffered from the first atmospheric correction schemes, which assumed no ocean contribution in the NIR, but improvements in the algorithms (e.g., *Siegel et al.* [2000] and *Patt et al.* [2003] for the SeaWiFS sensor) and possibly future enhanced sensor sensitivity should diminish this drawback.

[66] The use of the algorithms with remote-sensing data requires a better knowledge of the variations in the value of the $Q$ factor. In case 1 waters, the bidirectionality and its implications has been studied theoretically [*Morel and Gentili*, 1996]. It has also been measured at sea [*Morel et al.*, 1995; *Voss and Morel*, 2005]. In case 2 waters, the variations in $Q$ have been studied theoretically by *Loisel and Morel* [2001] but remain poorly documented. Recently, *Park and Ruddick* [2005] proposed a direct model to estimate the bidirectional variations of $R_{rs}$ when the IOPs are known in both case 1 and case 2 waters. Some additional efforts will be necessary to study the variations in $Q$ in an inverse model and to implement it in the future algorithms, on theoretical aspects and with the development of measurements.

[67] **Acknowledgments.** This work has been supported through a PhD fellowship to M. DORON with a CIFRE contract (Association Nationale de la Recherche Technique) and partly funded by the Service Hydrographique et Océanographique de la Marine (EPSHOM) and the ESA GMES Service Element Marcoast. The COASTlOOC project was funded by the Fourth Framework Program of the European Commission. We are grateful to Frank Fell, Vincent Fournier-Sicre, Grigor Obolensky, and Massimo Ferrari for their contribution to the COASTlOOC in situ measurements and data processing. We thank Simon Bélanger, Hervé Claustre, David Doxaran, and Yannick Huot for providing their optical data obtained during the campaigns CASES, PROSOPE, RSFlux, and Lunenburg Bay. We also thank Simon Bélanger, Emmanuel Boss, Annick Bricaud, Yannick

Huot, André Morel, and Mike Twardowski for their constructive comments on the first version of this paper.

## References


Austin, R. W., and T. J. Petzold (1981), The determination of the diffuse attenuation coefficient of sea water using the coastal zone color scanner, in *Oceanography From Space*, edited by J. F. R. Gower, Springer, New York.

Babin, M., and D. Stramski (2002), Light absorption by aquatic particles in the near-infrared spectral region, *Limnol. Oceanogr.*, *47*, 911–915.

Babin, M., A. Morel, V. Fournier-Sicre, F. Fell, and D. Stramski (2003a), Light scattering properties of marine particles in coastal and open ocean waters as related to the particle mass concentration, *Limnol. Oceanogr.*, *48*, 843–859.

Babin, M., D. Stramski, G. M. Ferrari, H. Claustre, A. Bricaud, G. Obolensky, and N. Hoepffner (2003b), Variations in the light absorption coefficients of phytoplankton, non-algal particles, and dissolved organic matter in coastal waters around Europe, *J. Geophys. Res.*, *108*(C7), 3211, doi:10.1029/2001JC000882.

Babin, M., and D. Stramski (2004), Variations in the mass-specific absorption coefficient of mineral particles suspended in water, *Limnol. Oceanogr.*, *49*, 756–767.

Barnard, A. H., W. S. Pegau, and J. R. V. Zaneveld (1998), Global relationships of the inherent optical properties of the oceans, *J. Geophys. Res.*, *103*(C11), 24955–24968, doi:10.1029/98JC01851.

Bélanger, S., H. Xie, N. Krotkov, P. Larouche, W. F. Vincent, and M. Babin (2006), Photomineralization of terrigenous dissolved organic matter in Arctic coastal waters from 1979 to 2003: Interannual variability and implications of climate change, *Global Biogeochem. Cycles*, *20*, GB4005, doi:10.1029/2006GB002708.

Boss, E., and W. S. Pegau (2001), The relationship of light scattering at an angle in the backward direction to the backscattering coefficient, *Appl. Opt.*, *40*, 5503–5507.

Boss, E., W. S. Pegau, M. Lee, M. Twardowski, E. Shybanov, G. Korotaev, and F. Baratange (2004), Particulate backscattering ratio at LEO 15 and its use to study particle composition and distribution, *J. Geophys. Res.*, *109*, C01014, doi:10.1029/2002JC001514.

Bricaud, A., A. Morel, and L. Prieur (1981), Absorption by dissolved organic matter of the sea (yellow substance) in the UV and visible domains, *Limnol. Oceanogr.*, *26*, 43–53.

Bricaud, A., and D. Stramski (1990), Spectral absorption coefficient of living phytoplankton and nonalgal biogenous matter: A comparison between the Peru upwelling area and the Sargasso Sea, *Limnol. Oceanogr.*, *35*, 562–582.

Claustre, H., A. Morel, S. B. Hooker, M. Babin, D. Antoine, K. Oubelkheir, A. Bricaud, K. Leblanc, B. Quéguiner, and S. Maritorena (2002), Is desert dust making oligotrophic waters greener?, *Geophys. Res. Lett.*, *29*(10), 1469, doi:10.1029/2001GL014056.

Defoin Platel, M., and M. Chami (2006), How ambiguous is the inverse problem of ocean color in coastal waters, *J. Geophys. Res.*, *112*, CO3004, doi:10.1029/2006JC003847.

Doxaran, D., M. Babin, and E. Leymarie (2006), Near-infrared light scattering by particles suspended in coastal waters. Presentation at Ocean Optics in Montréal, 2006.

Fournier, G. R., and J. L. Forand (1994), Analytic phase function for ocean water, in Ocean Optics XII, edited by J. S. Jaffe, *Proc. SPIE* 2258, 194–201.

Gordon, H. R., O. B. Brown, and M. M. Jacobs (1975), Computed relationship between the inherent and apparent optical properties of a flat homogeneous ocean, *Appl. Opt.*, *14*, 417–427.

Gould, R. W., R. A. Arnone, and P. M. Martinolich (1999), Spectral dependence of the scattering coefficient in Case 1 and Case 2 waters, *Appl. Opt.*, *38*, 2377–2383.

Huot, Y., C. A. Brown, and J. J. Cullen (2007), Retrieval of phytoplankton biomass from simultaneous inversion of reflectance, the diffuse attenuation coefficient, and sun-induced flourescence in coastal waters, *J. Geophys. Res.*, *112*, doi:10.1029/2006JC003794, in press.

International Ocean Color Coordinating Group (2006), Remote sensing of inherent optical properties: fundamentals, tests of algorithms, and applications, report number 5, edited by Z. P. Lee, Reports of the International Ocean Colour Coordinating Group No. 5, IOCCG, Dartmouth, Canada.

Lee, Z. P., and K. L. Carder (1994), Model for the interpretation of hyperspectral remote-sensing reflectance, *Appl. Opt.*, *33*, 5721–5732.

Lee, Z. P., K. L. Carder, T. G. Peacock, C. O. Davis, and J. L. Mueller (1996), Method to derive ocean absorption coefficients from remote-sensing reflectance, *Appl. Opt.*, *35*, 453–462.

Lee, Z. P., K. L. Carder, and R. Arnone (2002), Deriving inherent optical properties from water color: A multi-band quasi-analytical algorithm for optically deep waters, *Appl. Opt.*, *41*, 5755–5777.

Lee, Z. P., K. P. Du, and R. Arnone (2005a), A model for the diffuse attenuation coefficient of downwelling irradiance, *J. Geophys. Res.*, *110*, C02016, doi:10.1029/2004JC002275.

Lee, Z. P., M. Darecki, K. L. Carder, C. O. Davis, D. Stramski, and W. J. Rhea (2005b), Diffuse attenuation coefficient of downwelling irradiance: An evaluation of remote sensing methods, *J. Geophys. Res.*, *110*, C02017, doi:10.1029/2004JC002573.

Loisel, H., and A. Morel (2001), Non-isotropy of the upward radiance field in typical coastal (Case 2) waters, *Int. J. Remote Sens.*, *22*, 275–295.

Mobley, C. D. (1994), Light and Water: Radiative Transfer in Natural Waters, Elsevier, New York.

Mobley, C. D., B. Gentili, H. R. Gordon, Z. Jin, G. W. Kattawar, A. Morel, P. Reinersman, K. Stamnes, and R. H. Stavn (1993), Comparison of numerical models for computing underwater light fields, *Appl. Opt.*, *32*, 7484–7505.

Morel, A. (1974), Optical properties of pure water and pure seawater, in *Optical Aspects of Oceanography*, edited by N. G. Jerlov and E. S. Nielsen pp. 1–24, Elsevier, New York.

Morel, A., and L. Prieur (1977), Analysis of variations in ocean color, *Limnol. Oceanogr.*, *22*, 709–722.

Morel, A., and B. Gentili (1996), Diffuse reflectance of oceanic waters: III. Implications of bi-directionality for the remote-sensing problem, *Appl. Opt.*, *35*, 4850–4862.

Morel, A., and S. Maritorena (2001), Bio-optical properties of oceanic waters: A reappraisal, *J. Geophys. Res.*, *106*(C4), 7163–7180, doi:10.1029/2000JC000319.

Morel, A., K. J. Voss, and B. Gentili (1995), Bidirectional reflectance of oceanic waters: A comparison of modeled and measured upward radiance fields, *J. Geophys. Res.*, *100*, 13,143–13,150.

Morel, A., B. Gentili, H. Claustre, M. Babin, A. Bricaud, J. Ras, and F. Tieche (2007), Optical properties of the clearest natural waters, *Limnol. Oceanogr.*, *52*(1), 217–229.

Mueller, J. L. (2000), SeaWiFS algorithm for the diffuse attenuation coefficient, K (490), using water-leaving radiances at 490 and 555 nm, in *SeaWiFS Postlaunch Calibration and Validation Analyses*, part 3, edited by S. B. Hooker, pp. 24–27, NASA Goddard Space Flight Center, Greenbelt, Md.

Mueller, J. L., and R. W. Austin (1995), Ocean optics protocols for SeaWiFS validation, revision 1, NASA Tech. Memo. 104566, vol. 25, edited by S. B. Hooker, E. R. Firestone, and J. G. Acker, pp. 66, NASA Goddard Space Flight Center, Greenbelt, Md.

Park, Y.-J., and K. Ruddick (2005), Model of remote-sensing reflectance including bidirectional effects for case 1 and case 2 waters, *Appl. Opt.*, *44*, 1236–1248.

Patt, F. S., et al. (2003), Algorithm Updates for the Fourth SeaWiFS Data Reprocessing, NASA Tech. Memo. 2003-206892, vol. 22, 74 pp., edited by S. B. Hooker and E. R. Firestone, NASA Goddard Space Flight Center, Greenbelt, Md.

Pope, R., and E. Fry (1997), Absorption spectrum (380–700 nm) of pure water: II. Integrating cavity measurements, *Appl. Opt.*, *36*, 8710–8723.

Preisendorfer, R. W. (1986), Secchi disk science: Visual optics of natural waters, *Limnol. Oceanogr.*, *31*, 909–926.

Roesler, C. S., and E. Boss (2003), Spectral beam attenuation coefficient retrieved from ocean color inversion, *Geophys. Res. Lett.*, *30*(9), 1468, doi:10.1029/2002GL016185.

Roesler, C. S., and M. J. Perry (1995), In situ phytoplankton absorption, fluorescence emission and particulate backscattering spectra determined from reflectance, *J. Geophys. Res.*, *100*(C7), 13279–13294, doi:10.1029/95JC00455.

Ruddick, K. G., H. J. Gons, M. Rijkeboer, and G. Tilstone (2001), Optical remote sensing of chlorophyll a in Case 2 waters by use of an adaptive two-band algorithm with optimal error properties, *Appl. Opt.*, *40*, 3575–3585.

Sathyendranath, S., L. Prieur, and A. Morel (1989), A three-component model of ocean color and its application to remote sensing of phytoplankton pigments in coastal waters, *Int. J. Remote Sens.*, *10*, 1373–1394.

Siegel, D. A., M. Wang, S. Maritorena, and W. Robinson (2000), Atmospheric correction of satellite ocean color imagery: The black pixel assumption, *Appl. Opt.*, *39*, 3582–3591.

Simis, S. G. H., S. W. M. Peters, and H. J. Gons (2005), Remote sensing of the cyanobacterial pigment phycocyanin in turbid waters, *Limnol. Oceanogr.*, *50*, 237–245.

Stramski, D., E. Boss, D. Bogucki, and K. J. Voss (2004), The role of seawater constituents in light backscattering in the ocean, *Prog. Oceanogr.*, *61*, 27–56.

Sullivan, J. M., M. S. Twardowski, P. L. Donaghay, and S. A. Freeman (2005), Use of optical scattering to discriminate particle types in coastal waters, *Appl. Opt.*, *44*, 1667–1680.

Sullivan, J. M., M. S. Twardowski, J. R. V. Zaneveld, C. M. Moore, A. H. Barnard, P. L. Donaghay, and B. Rhoades (2006), Hyperspectral

temperature and salt dependencies of absorption by water and heavy water in the 400–750 n spectral range, *Appl. Opt.*, *45*, 5294–5309.

Sydor, M., R. W. Gould, R. A. Arnone, V. I. Haltrin, and W. Goode (2004), Uniqueness in remote sensing of the inherent optical properties of ocean water, *Appl. Opt.*, *43*, 2156–2162.

Tassan, S., and G. M. Ferrari (2003), Variability of light absorption by aquatic particles in the near-infrared spectral region, *Appl. Opt.*, *42*, 4802–4810.

Twardowski, M. S., E. Boss, J. B. Macdonald, W. S. Pegau, A. H. Barnard, and J. R. V. Zaneveld (2001), A model for estimating bulk refractive index from the optical backscattering ratio and the implications for understanding particle composition in case I and case II waters, *J. Geophys. Res.*, *106*(C7), 14129–14142, doi:10.1029/2000JC000404.

Tyler, J. E. (1968), The Secchi disc, *Limnol. Oceanogr.*, *13*, 1–6.

Voss, K., and A. Morel (2005), Bidirectional reflectance function for oceanic waters with varying chlorophyll concentration: Measurements versus predictions, *Limnol. Oceanogr.*, *50*, 698–705.

Zaneveld, J. R. V., and W. S. Pegau (2003), Robust underwater visibility parameter, *Opt. Express*, *11*, 2997–3009.

M. Babin, Laboratoire d'Océanographie de Villefranche, CNRS, 06230, Villefranche-sur-Mer, France.

M. Doron, O. Hembise, and A. Mangin, ACRI-ST, 260 route du Pin Montard, B.P. 234, 06904, Sophia Antipolis, France. (doron@obs-vlfr.fr)